Nanoscale flexoelectric energy harvesting

Qian Deng [a], Mejdi Kammoun [a], Alper Erturk [b], Pradeep Sharma [a,c,*]

[a] Department of Mechanical Engineering, University of Houston, Houston, TX 77204, USA
[b] G. W. Woodruff School of Mechanical Engineering, Georgia Institute of Technology, Atlanta, GA, USA
[c] Department of Physics, University of Houston, Houston, TX 77204, USA

A B S T R A C T

One of the most tantalizing applications of piezoelectricity is to harvest energy from ambient mechanical vibrations for powering micro and nano devices. However, piezoelectricity is restricted only to certain materials and is severely compromised at high temperatures. In this article, we examine in detail, the possibility of using the phenomenon of *flexoelectricity* for energy harvesting. The flexoelectric effect is universally present in *all* dielectrics and exhibits a strong scaling with size. Using a simple beam-based paradigmatical design, we theoretically and computationally examine flexoelectric energy harvesting under harmonic mechanical excitation. We find that the output power density and conversion efficiency increase significantly when the beam thickness reduces from micro to nanoscale and flexoelectricity-based energy harvesting can be a viable alternative to piezoelectrics. Specifically, the conversion efficiency in flexoelectric transduction at sub-micron thickness levels is observed to increase by two orders of magnitude as the thickness is reduced by an order of magnitude. The flexoelectric energy harvester works even for a single layer beam with a symmetric cross section which is not possible in piezoelectric energy harvesting. Our results also pave the way for exploration of high temperature energy harvesting since unlike piezoelectricity, flexoelectricity persists well beyond the Curie temperatures of the high electromechanical coupling ferroelectrics that are often used.

© 2014 Elsevier Ltd. All rights reserved.

1. Introduction

Harvesting ambient waste energy into usable energy has received increasing attention over the last few years (Hudak and Amatucci, 2008; Elvin and Erturk, 2013). Efficient conversion of the ubiquitous ambient mechanical vibrations to electric energy for the powering of micro and nano systems, without the use of batteries, is an intensely researched subject. In particular, piezoelectric materials, as transducers between mechanical and electrical stimuli, are usually considered to be the ideal choice for such energy harvesting due to their high power density and ease of application (Anton and Sodano, 2007; Cook-Chennault et al., 2008; Priya, 2007). The applications of piezoelectric energy harvesting range from shoe-mounted inserts (Kymissis et al., 1998; Shenck and Paradiso, 2001) to unmanned aerial vehicles (Anton et al., 2012). Micro and nano implementations of piezoelectric energy harvesting have also received growing attention in the last few years due to the developments in ferroelectric thin films for MEMS (Trolier-McKinstry and Muralt, 2004; Jeon, 2005;

Muralt et al., 2009) and non-ferroelectric nano wires NEMS (Wang and Song, 2006; Xu et al., 2010).

Recently, a somewhat understudied electromechanical coupling, *flexoelectricity*, has attracted a fair amount of attention from both fundamental and applications points of view leading to intensive experimental (Cross, 2006; Ma and Cross, 2001, 2002, 2003, 2006; Catalan et al., 2004; Zubko et al., 2007; Fu et al., 2006, 2007) and theoretical work (Sharma et al., 2007; Majdoub et al., 2009a; Eliseev et al., 2009, 2011; Maranganti and Sharma, 2009; Majdoub et al., 2008a,b, 2009b,c; Sharma et al., 2010, 2012; Gharbi et al., 2011; Kalinin and Meunier, 2008; Dumitrica et al., 2002). Piezoelectricity is restricted to only certain crystal structures and refers to a linear coupling between the development of polarization due to the action of *uniform* deformation and vice versa. In contrast, flexoelectricity links strain gradients to polarization and, in principle, exists in *all* dielectrics. In other words, even in non-piezoelectric materials, strain gradients can lead to the development of polarization. This effect is generally small but symmetry allows for its universal presence—unlike piezoelectricity. The reader is referred to the following articles for a detailed review: Refs. Tagantsev (1986, 2009), Maranganti et al. (2006), Nguyen et al. (2013) and Eliseev et al. (2011). Since strain gradient scales with feature size, and high values are easily obtainable at

small length scales, flexoelectricity is expected to be significant at the micro and nanoscale possibly outperforming piezoelectricity in several scenarios. It is worth while to point out that flexoelectricity appears to have several ramifications for biophysics as well. For example, electromechanical transduction related to mammalian hearing appear to be dictated by flexoelectricity of biological membranes (Brownell et al., 2001, 2003; Raphael et al., 2000).

A commonly encountered problem in piezoelectric devices is *electric fatigue*. It is found that the switching polarization decreases significantly in some piezoelectric materials after some switching cycles (Jiang et al., 1994). Although the mechanism for this fatigue is still not full understood, some possible causes includes: transition of internal structure into a more stable configuration (Quarrie, 1953), the appearance of microcracks (Carl, 1975; Salaneck, 1972), and structural inhomogeneity which reduce the domain wall mobility (Williams, 1965). Since flexoelectricity allows a broader range of choices for the material, we can carefully choose those materials with higher fatigue resistance.

In this paper, we propose a flexoelectric energy harvester which shares some similarities but is, in many ways, quite different from the piezoelectric counterparts. The flexoelectric energy harvester is simpler in structure, allows a broader range of materials choice and exhibits strong size-scaling making it ideal for some micro scale and possibly all nanoscale applications. In Section 2, we present the main formulation and derive the requisite governing equations. In Section 3, we solve the simplest possible energy harvesting problem assuming harmonic base excitation. Based on the solution, the performance of the flexoelectric energy harvester is analyzed in Section 4. In particular, the size effect is studied in detail.

2. Electroelastic system and mathematical formulation

The flexoelectric energy harvester configuration investigated in this work is shown in Fig. 1. The flexoelectric cantilever beam is coated by perfectly conductive electrodes on its top and bottom surfaces. We assume that the electrode layers are very thin so that their contribution to the vibration of the cantilever can be neglected while their presence can easily be incorporated by preserving the centrosymmetry. The coordinate system and the resulting position coordinates x_1, x_2, x_3 are shown in Fig. 1. The longitudinal axis is denoted by x_1. The cantilever beam is mounted to a base moving in the x_3 direction. The transverse base displacement is denoted by $w_b(t)$. Due to the movement of the base, the cantilever beam undergoes bending vibrations. Dynamic strain gradient associated with vibration results in an alternating potential difference across the electrodes. The electrodes are connected to a resistive load (R) to quantify the electrical power output. Although the internal resistance of the dielectric beam is not taken into account, it can easily by considered as a resistor connected in parallel to the load resistance.

2.1. Variational principle for flexoelectricity

There are several approaches for formulating the electromechanical coupling in deformable materials. A particularly elegant
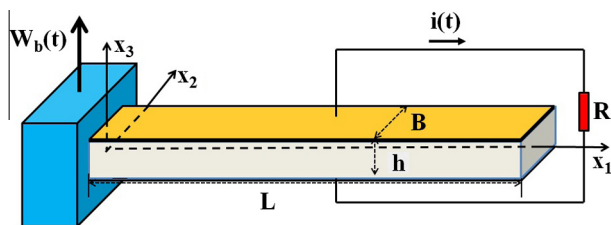

Fig. 1. A centrosymmetric flexoelectric energy harvester under base excitation.

exposition has been recently presented by Liu (2014). Based on Liu's work, Deng et al. (2014) studied the flexoelectricity in softmaterials. Other insightful works and alternative ways of formulating electrostatics of deformable bodies may also be referred to Dorfmann and Ogden (2005), McMeeking and Landis (2005), Suo et al. (2008), Steigmann (2009), Eringen and Maugin (1990) and Toupin (1956). Since the majority of the literature on linear active materials (such as piezoelectric dielectrics) follows Mindlin's approach (Mindlin, 1961, 1968; Tiersten, 1967), we have followed likewise.

Neglecting fringe fields, the variational principle for flexoelectric body can be written in the following form:

$$\delta \int_{t_1}^{t_2} dt \int_V \left[\frac{1}{2}\rho|\dot{\mathbf{u}}^m|^2 - \left(W^L - \frac{1}{2}\epsilon_0|\nabla\phi|^2 + \mathbf{P}\cdot\nabla\phi \right) \right] dV$$
$$+ \int_{t_1}^{t_2} dt \int_V \left(\mathbf{q}\cdot\delta\mathbf{u}^m + \mathbf{E}^0\cdot\delta\mathbf{P} \right) dV + \int_{t_1}^{t_2} dt \int_{\partial V} \tilde{D}\delta\phi dA = 0 \quad (1)$$

where $\mathbf{u}^m$ and ϕ are the absolute displacement and potential field in the beam, $\mathbf{P}$ is the polarization density, W^L is the internal energy density, $\mathbf{q}$ and $\mathbf{E}^0$ correspond to the external body force and the external electric field, respectively. Because of the conductive electrodes coated on the surface, a boundary integration term is added here. This last term corresponds to the virtual work done by moving charges on to or out of the electrodes as a product of the variation of potential ϕ and the average electric displacement $\tilde{D}$. Note that the bulk electric displacement is related to the polarization by $-\epsilon_0\nabla\phi + \mathbf{P}$.

At the outset we assume a linearized setting. Then the internal energy density W^L can be written as (Sahin and Dost, 1988; Sharma et al., 2007)

$$W^L = \frac{1}{2}\mathbf{P}\cdot\mathbf{aP} + \frac{1}{2}\mathbf{S}\cdot\mathbf{cS} + \mathbf{P}\cdot\mathbf{dS} + \mathbf{P}\cdot\mathbf{f}\nabla\nabla\mathbf{u} + \frac{1}{2}\nabla\nabla\mathbf{u}\cdot\mathbf{g}\nabla\nabla\mathbf{u} \quad (2)$$

where $\mathbf{u}$ is the displacement field relative to the moving base $\mathbf{u} = \{u_1^m, u_2^m, u_3^m - w_b(t)\}^T$, $\mathbf{S} = \frac{1}{2}(\nabla\mathbf{u} + (\nabla\mathbf{u})^T)$ is the infinitesimal strain tensor, and $\nabla\nabla\mathbf{u}$ is the strain gradient tensor. The coefficients $\mathbf{a}, \mathbf{c}, \mathbf{d}, \mathbf{f}$, and $\mathbf{g}$ are material properties, i.e., $\mathbf{a}$ is the reciprocal dielectric susceptibility which relates to relative permittivity ϵ_r and the vacuum permittivity ϵ_0 by $\mathbf{a} = \frac{1}{(\epsilon_r-1)\epsilon_0}$, $\mathbf{c}$ corresponds to elastic modulus, $\mathbf{d}$ and $\mathbf{f}$ are the piezoelectric and flexoelectric constants, respectively. The parameter $\mathbf{g}$ is nonzero only if the strain gradient is considered. $\mathbf{g}$ relates strain gradient $\nabla\nabla\mathbf{u}$ to its energy conjugate, high order stress tensor (Majdoub et al., 2008a).

The base movement $w_b(t)$ is the given Dirichlet boundary condition, so we have $\delta\mathbf{u}^m = \delta\mathbf{u}$. For independent $\mathbf{P}, \mathbf{u}$, and ϕ, we have

$$\delta \int_{t_1}^{t_2} dt \int_V \left[W^L - \frac{1}{2}\epsilon_0|\nabla\phi|^2 + \mathbf{P}\cdot\nabla\phi \right] dV = \int_{t_1}^{t_2} dt$$
$$\int_V \left[\frac{\partial W^L}{\partial \mathbf{P}}\delta\mathbf{P} + \frac{\partial W^L}{\partial \mathbf{S}}\delta\mathbf{S} + \frac{\partial W^L}{\partial \nabla\nabla\mathbf{u}}\delta(\nabla\nabla\mathbf{u}) - \epsilon_0\nabla\phi\delta(\nabla\phi) + \mathbf{P}\delta(\nabla\phi) + \nabla\phi\delta\mathbf{P} \right] dV \quad (3)$$

and

$$\delta \int_{t_1}^{t_2} dt \int_V \frac{1}{2}\rho|\ddot{\mathbf{u}}^m|^2 dV = -\int_{t_1}^{t_2} dt \int_V \rho\ddot{\mathbf{u}}^m\delta\mathbf{u} dV$$

Then, from Eq. (1), we have the Euler–Lagrange equations

$$Div\left[\frac{\partial W^L}{\partial \mathbf{S}} - Div\left(\frac{\partial W^L}{\partial \nabla\nabla\mathbf{u}} \right) \right] + \mathbf{q} = \rho\ddot{\mathbf{u}}^m$$

$$\frac{\partial W^L}{\partial \mathbf{P}} + \nabla\phi = \mathbf{E}^0 \quad (4)$$

$$Div(-\epsilon_0\nabla\phi + \mathbf{P}) = 0$$

in the domain V and the corresponding boundary conditions

$$(-\epsilon_0 \nabla \phi + \mathbf{P}) \cdot \mathbf{N} = \widetilde{D}$$

$$\left[\frac{\partial W^L}{\partial \mathbf{S}} - Div\left(\frac{\partial W^L}{\partial \nabla \nabla \mathbf{u}} \right) \right] \cdot \mathbf{N} = 0 \qquad (5)$$

$$\left(\frac{\partial W^L}{\partial \nabla \nabla \mathbf{u}} \right) \cdot \mathbf{N} = 0$$

on its boundary Γ. Where $\mathbf{N}$ is the direction normal to Γ and $\widetilde{D}$ is the average electric displacement.

2.2. Flexoelectric Euler–Bernoulli beam model

The deformation of the cantilever beam is assumed to be small. To illustrate the central ideas of flexoelectric energy harvesting, we use the Euler–Bernoulli model. The key conclusions, that we are interested in emphasizing in this work, are unlikely to be affected by this assumption. Future works may consider more sophisticated beam-assumptions, in particular nonlinear effects. The relative displacement field in the Euler–Bernoulli model is:

$$\mathbf{u} = \left\{ -x_3 \frac{\partial w(x_1,t)}{\partial x_1}, 0, w(x_1,t) \right\}^T \qquad (6)$$

where $w(x_1,t)$ is the transverse displacement of the neutral surface at point x_1 and time t. From this displacement field, the normal strain in x_1 direction is the only non-zero strain component which can be written as

$$S_{11} = -x_3 \frac{\partial^2 w}{\partial x_1^2} \qquad (7)$$

The non-zero strain gradient components are

$$S_{11,1} = -x_3 \frac{\partial^3 w}{\partial x_1^3}, \quad S_{11,3} = -\frac{\partial^2 w}{\partial x_1^2} \qquad (8)$$

where $S_{11,1}$ is small as compared to $S_{11,3}$ due to the thin beam assumption. Therefore the component $S_{11,1}$ is ignored in the present work.

Generally, strain gradient $S_{11,3}$ will induce the separation of positive and negative charge centers. A schematic representation for the polarization induced by strain gradient is shown in Fig. 2. The blue and red particles represent the negative and positive material particles in a unit cell. As can be seen from Fig. 2, after deformation, the induced polarization is generated along the x_3 direction. The polarization density field within the cantilever beam has the following form:

$$\mathbf{P}(x_1, x_3, t) = \{0, 0, P(x_1, x_3, t)\}^T \qquad (9)$$

Given the above assumptions, and settings $a = a_{33}$, $c = c_{1111}$, $d = d_{311}$, $f = f_{3113}$, and $g = g_{113113}$, the internal energy density W^L is rewritten as:

$$W^L = \frac{1}{2} aP^2 + \frac{1}{2} c x_3^2 \left(\frac{\partial^2 w}{\partial x_1^2} \right)^2 - d x_3 P \frac{\partial^2 w}{\partial x_1^2} - fP \frac{\partial^2 w}{\partial x_1^2}$$
$$+ \frac{1}{2} g \left(\frac{\partial^2 w}{\partial x_1^2} \right)^2 \qquad (10)$$

Using the above expression for internal energy density, the left hand side of Eq. (3) can be written as

$$\int_{t_1}^{t_2} dt \int_V \left[aP\delta P + c x_3^2 \frac{\partial^2 w}{\partial x_1^2} \delta\left(\frac{\partial^2 w}{\partial x_1^2} \right) - d x_3 P \delta\left(\frac{\partial^2 w}{\partial x_1^2} \right) \right.$$
$$- d x_3 \frac{\partial^2 w}{\partial x_1^2} \delta P - fP \delta\left(\frac{\partial w}{\partial x_1^2} \right) - f \frac{\partial^2 w}{\partial x_1^2} \delta P + g \frac{\partial^2 w}{\partial x_1^2} \delta\left(\frac{\partial^2 w}{\partial x_1^2} \right)$$
$$\left. -\epsilon_0 \frac{\partial \phi}{\partial x_3} \delta\left(\frac{\partial \phi}{\partial x_3} \right) - \epsilon_0 \frac{\partial \phi}{\partial x_1} \delta\left(\frac{\partial \phi}{\partial x_1} \right) + P \delta\left(\frac{\partial \phi}{\partial x_3} \right) + \frac{\partial \phi}{\partial x_3} \delta P \right] dV \qquad (11)$$
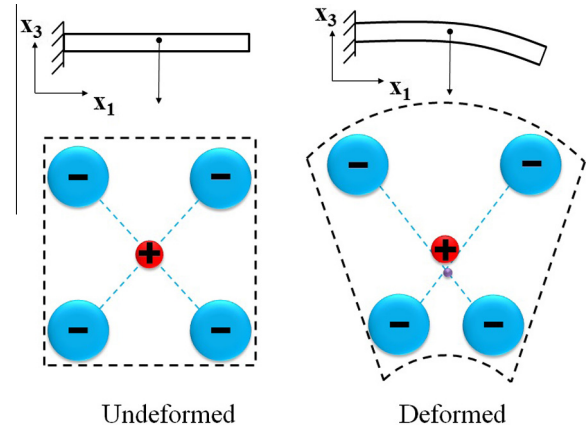

Fig. 2. Polarization due to bending of a centrosymmetric beam. (For interpretation of the references to colour in this figure caption, the reader is referred to the web version of this article.)

There are no external body forces or electric fields in the present work. Then (1) can be further written as

$$\int_{t_1}^{t_2} dt \int_V \rho(\ddot{w} + \ddot{w}_b) \delta w dV + \int_{t_1}^{t_2} dt \int_V \left[\left(aP - d x_3 \frac{\partial^2 w}{\partial x_1^2} - f \frac{\partial^2 w}{\partial x_1^2} + \frac{\partial \phi}{\partial x_3} \right) \delta P \right.$$
$$+ \left(c x_3^2 \frac{\partial^2 w}{\partial x_1^2} - d x_3 P - fP + g \frac{\partial^2 w}{\partial x_1^2} \right) \delta\left(\frac{\partial^2 w}{\partial x_1^2} \right) + \left(P - \epsilon_0 \frac{\partial \phi}{\partial x_3} \right) \delta\left(\frac{\partial \phi}{\partial x_3} \right)$$
$$\left. + \left(-\epsilon_0 \frac{\partial \phi}{\partial x_1} \right) \delta\left(\frac{\partial \phi}{\partial x_1} \right) \right] dV = 0 \qquad (12)$$

where the kinetic energy contribution from the rotary inertia is neglected. It should also be noted that the mechanical dissipation mechanism will be included later in the form of proportional damping whereas dielectric losses are neglected in this framework.

In the above equation, δP is arbitrary, so we have

$$aP - d x_3 \frac{\partial^2 w}{\partial x_1^2} - f \frac{\partial^2 w}{\partial x_1^2} + \frac{\partial \phi}{\partial x_3} = 0 \qquad (13)$$

Substituting Eq. (13) into the above variational equation and changing the volume integration $\int_V$ into $\int_0^L \int_A$ (A is the cross section of the beam), we obtain the following variational equation without the polarization density P:

$$\int_{t_1}^{t_2} dt \int_0^L \rho A_P (\ddot{w} + \ddot{w}_b) \delta w dx_1 + \int_{t_1}^{t_2} dt \int_0^L \left\{ \left[\left(c - \frac{d^2}{a} \right) \right. \right.$$
$$\left. I_P - \frac{2df}{a} H_P - \left(\frac{f^2}{a} - g \right) A_P \right] \frac{\partial^2 w}{\partial x_1^2} - \int_A \left(\frac{d}{a} x_3 + \frac{f}{a} \right) \frac{\partial \phi}{\partial x_3} dS \right\} \delta\left(\frac{\partial^2 w}{\partial x_1^2} \right) dx_1 = 0$$

where $(A_P, H_P, I_P) = \int_A (1, x_3, x_3^2) dA$ and H_P vanishes for a structure that is symmetric with respect to the neutral axis (x_1-axis) of the beam. Furthermore we define the effective bending rigidity $(EI)^* = \left(c - \frac{d^2}{a} \right) I_P - \frac{2df}{a} H_P - \left(\frac{f^2}{a} - g \right) A_P$ which describes the resistance of the flexoelectric beam to bending. A limitation in the linear framework is that, beyond a certain critical point the effective bending rigidity may turn negative. Future work may consider a nonlinear framework to alleviate this issue. The present work uses the geometrically and electroelastically linear framework to explore the basic phenomena within the applicable range.

It is worthwhile to mention that, in reality, ϕ is a function of both time t and the coordinates x_1, x_3. However, since there are no free charges inside the beam and the beam considered here is very thin, it is reasonable to assume that the self-field inside the beam is independent of the spatial coordinates implying that $E_3 = -\frac{\partial \phi}{\partial x_3} = const.$ at an arbitrary instant of time. Given the top and bottom electrode boundary conditions, we further have $E_3 = -v(t)/h$ where $v(t)$ is

the potential difference between the two conductive electrodes. For the same reason, we also have $E_1 = -\frac{\partial \phi}{\partial x_1} = 0$ at the top and bottom surfaces. So, for the thin beam case, it is reasonable to assume $E_1 = 0$ through out the whole beam. Under these linear assumptions, we can rewrite the above equation as

$$\int_{t_1}^{t_2} dt \int_0^L \rho A_P(\ddot{w} + \ddot{w}_b)\delta w \, dx_1 + \int_{t_1}^{t_2} dt$$
$$\int_0^L \left\{ \left[\left(c - \frac{d^2}{a}\right)I_P - \frac{2df}{a}H_P - \left(\frac{f^2}{a} - g\right)A_P \right] \frac{\partial^2 w}{\partial x_1^2} - \left(\frac{d}{a}H_P + \frac{f}{a}A_P\right)\frac{v(t)}{h} \right\}$$
$$\delta\left(\frac{\partial^2 w}{\partial x_1^2}\right)dx_1 = 0 \tag{14}$$

The current $i(t)$ flows through the resistor R must be equal to the time rate of change of the average electric displacement $\bar{D}_3 = \frac{1}{h}\int_V D_3 dV$, resulting in the electrical circuit equation with flexoelectric coupling:

$$i(t) = \frac{v(t)}{R} = \frac{1}{h}\frac{d}{dt}\int_V \left(-\epsilon_0 \frac{v(t)}{h} + P\right)dV$$
$$= -\frac{BL}{h}\left(\epsilon_0 + \frac{1}{a}\right)\dot{v}(t) + \frac{1}{h}\int_0^L \left(\frac{d}{a}H_P + \frac{f}{a}A_P\right)\frac{\partial^2 \dot{w}}{\partial x_1^2}dx_1 \tag{15}$$

3. Solution and frequency response

We adopt the assumed-modes method (Erturk and Inman, 2011; Erturk, 2012) to solve the energy harvesting problem posed in the preceding section. The assumed-modes method employs a series discretization approach that is similar to the Rayleigh–Ritz method (Meirovitch, 2001). In fact these two techniques yield the same results for the same admissible functions. The distributed-parameter variable in the mechanical domain is $w(x_1, t)$ whereas the electrical variable is $v(t)$. The following finite series is used to represent the mechanical response of the beam:

$$w(x_1, t) = \sum_{k=1}^N a_k(t)\xi_k(x_1) \tag{16}$$

where N is the number of modes used in the series discretization, $\xi_k(x_1)$ are the kinematically admissible trial functions which satisfy the essential boundary conditions, while $a_k(t)$ are unknown generalized coordinates. If the problem has an exact solution, the eigenfunctions are available (as in the uniform cross-section cantilever case shown in Fig. 1 and studied in this work), the admissible functions can be taken as the eigenfunctions and convergence is not an issue. However, for problems with no exact solution (such as a varying cross-section problem), sufficient number (N) of admissible functions must be used to ensure convergence.

For the symmetric Euler–Bernoulli cantilever beam studied here, the trial function is taken to be the eigenfunction (Erturk and Inman, 2009, 2011) is given by

$$\xi_k(x_1) = \cos\frac{\lambda_k}{L}x_1 - \cosh\frac{\lambda_k}{L}x_1 + \frac{\sin\lambda_k - \sinh\lambda_k}{\cos\lambda_k + \cosh\lambda_k}\left(\sin\frac{\lambda_k}{L}x_1 - \sinh\frac{\lambda_k}{L}x_1\right) \tag{17}$$

where λ_k is the kth root of the transcendental characteristic equation

$$1 + \cos\lambda\cosh\lambda = 0$$

Substituting the series representation Eq. (16) into Eqs. (14) and (15), the discrete Euler–Lagrange equations for the structurally undamped Euler–Bernoulli beam model are obtained as

$$\mathbf{M}\ddot{\mathbf{a}}(t) + \mathbf{K}\mathbf{a}(t) - (\Theta^p + \Theta^f)v(t) = \bar{\mathbf{f}}$$
$$C_f\dot{v}(t) + \frac{v(t)}{R} + (\Theta^p + \Theta^f)^T\dot{\mathbf{a}}(t) = 0 \tag{18}$$

where

$$M_{kl} = \rho A_P \int_0^L \xi_k(x_1)\xi_l(x_1)dx_1$$

$$K_{kl} = (EI)^* \int_0^L \xi_k''(x_1)\xi_l''(x_1)dx_1$$

$$\theta_l^p = \frac{1}{h}\frac{d}{a}H_P \int_0^L \xi_l''(x_1)dx_1$$

$$\theta_l^f = \frac{1}{h}\frac{f}{a}A_P \int_0^L \xi_l''(x_1)dx_1$$

$$\bar{f}_l = -\ddot{w}_b(t)\int_0^L \rho A_P\xi_l(x_1)dx_1$$

are the components of $\mathbf{M}, \mathbf{K}, \Theta^p, \Theta^f$, and $\bar{\mathbf{f}}$, respectively. The parameter C_f is given by

$$C_f = \frac{BL}{h}\left(\epsilon_0 + \frac{1}{a}\right)$$

Since the focus in energy harvesting is placed on the resonance behavior (i.e. damping controlled region), it is necessary to account for structural dissipation in the system. In this work, we resort to Rayleigh damping which is proportional to the mass and the stiffness matrices. We introduce the damping matrix $\mathbf{D}$ with

$$\mathbf{D} = \mu\mathbf{M} + \gamma\mathbf{K}$$

where μ and γ are constants of proportionality which can be calculated using two modal damping ratios, ζ_1 and ζ_2 through the following equation (Clough and Penzien, 1993):

$$\begin{bmatrix} \gamma \\ \mu \end{bmatrix} = \frac{2\omega_1\omega_2}{\omega_1^2 - \omega_2^2}\begin{bmatrix} \frac{1}{\omega_2} & -\frac{1}{\omega_1} \\ -\omega_2 & \omega_1 \end{bmatrix}\begin{bmatrix} \zeta_1 \\ \zeta_2 \end{bmatrix}$$

where ω_1 and ω_2 are the first two nature frequencies of the beam. In the absence of other damping mechanisms, the damping ratio is related to the material quality factor ($Q = 1/2\zeta$).

With the consideration of Rayleigh damping, the Euler–Lagrange equations (18) are written as

$$\mathbf{M}\ddot{\mathbf{a}}(t) + \mathbf{D}\dot{\mathbf{a}}(t) + \mathbf{K}\mathbf{a}(t) - (\Theta^p + \Theta^f)v(t) = \bar{\mathbf{f}}$$
$$C_f\dot{v}(t) + \frac{v(t)}{R} + (\Theta^p + \Theta^f)^T\dot{\mathbf{a}}(t) = 0 \tag{19}$$

Note that the coupling vectors Θ^p and Θ^f are parameters corresponding to the piezoelectricity and the flexoelectricity of the material, respectively. They couple the mechanical and electrical behaviors of the cantilever beam. The two Euler–Lagrange equations in (18) or (19) would be decoupled if both Θ^p and Θ^f are zero. For a symmetric cross section beam with respect to the neutral axis (x_1-axis), Θ^p equals to zero since $H_P = 0$. Therefore the flexoelectric term Θ^f is important as the major source of electromechanical coupling in such centrosymmetric beams. However, the flexoelectric effect is too slight to be detected at macroscale. In the next section of this paper, we show that the significance of flexoelectricity changes with the sample size which throw light on the energy harvesting for MEMS and NEMS applications.

If the base vibration is harmonic of the form, $w_b(t) = W_0 e^{j\omega t}$, then the force vector $\bar{\mathbf{f}}$ becomes

$$\bar{\mathbf{f}} = \mathbf{F}e^{j\omega t} \tag{20}$$

where

$$F_k = W_0\omega^2 \int_0^L \rho A_P\xi_k(x_1)dx_1$$

Since the base vibration is harmonic and the system is assumed to be linear, it is reasonable to assume that the steady-state response of the system is also harmonic with the same frequency ω. Therefore the generalized coordinate $\mathbf{a}(t)$ and output voltage $v(t)$ can be expressed as the following harmonic forms

$$\mathbf{a}(t) = \mathbf{A}e^{j\omega t}, \quad v(t) = Ve^{j\omega t}$$

Using the above assumption, the solution is reduced to solving a set of algebraic equations (19). They are given by

$$[-\omega^2 \mathbf{M} + j\omega(\mu\mathbf{M} + \gamma\mathbf{K}) + \mathbf{K}]\mathbf{A} - \mathbf{\Theta}V = \mathbf{F} \tag{21}$$

$$\left(j\omega C_f + \frac{1}{R}\right)V + j\omega\mathbf{\Theta}^T\mathbf{A} = 0 \tag{22}$$

where $\mathbf{\Theta} = \mathbf{\Theta}^p + \mathbf{\Theta}^f$ is the total coupling term and is equal to $\mathbf{\Theta}^f$ for a centrosymmetric beam (a beam that is symmetric with respect to x_1-x_2 surface in Fig. 1).

Then the complex-valued unknowns $\mathbf{A}$ and V are obtained through solving the above linear algebraic equations

$$V = j\omega\left(j\omega C_f + \frac{1}{R}\right)^{-1}(-\mathbf{\Theta}^T)$$

$$\left[-\omega^2\mathbf{M} + j\omega(\mu\mathbf{M} + \gamma\mathbf{K}) + \mathbf{K} + j\omega\left(j\omega C_f + \frac{1}{R}\right)^{-1}\mathbf{\Theta}\mathbf{\Theta}^T\right]^{-1}\mathbf{F} \tag{23}$$

$$\mathbf{A} = \left[-\omega^2\mathbf{M} + j\omega(\mu\mathbf{M} + \gamma\mathbf{K}) + \mathbf{K}\right]^{-1}(\mathbf{F} + \mathbf{\Theta}V) \tag{24}$$

which contain both the amplitude and phase information of the voltage across the electrical load and flexoelectrically shunted vibration response. Note that the $\mathbf{A}$ vector is the vector of generalized coordinates and it is the back substitution of Eq. (24) into Eq. (16) that yields the physical vibration response $w(x_1, t)$.

4. Case study and results

In this section, the electromechanical behavior of the proposed flexoelectric energy harvester under harmonic base excitation is simulated using the continuum framework and its assumed-modes solution. We choose polyvinylidene difluoride (PVDF) as the model material system which has the following properties: $a = \frac{1}{(\epsilon_r - 1)\epsilon_0} = 1.38 \times 10^{10}$ Nm^2/C^2 where $\epsilon_r = 9.2$ is the relative permittivity of PVDF (Chu and Salem, 2012) and $\epsilon_0 = 8.854 \times 10^{-12}$ C^2/(Nm^2); $f = -a\mu'_{12} = -179$ Nm/C is calculated from the flexoelectric coefficient $\mu'_{12} = 1.3 \times 10^{-10}$ C/m (Chu and Salem, 2012); For PVDF, $c = 3.7$ GPa is the Young's modulus (Guney, 2005); It is known that $\sqrt{g/c}$ is of the same order of the radius of gyration of PVDF, so we chose $g = 5 \times 10^{-7}$ N for the current work; $\rho = 1.78 \times 10^3$ kg/m^3 is the density of PVDF; $d = -1.02 \times 10^9$ N/C is obtained from the piezoelectric coefficient $d_{31} = 20$ pm/V (Murayama et al., 1976) by $d = -cad_{31}$; The damping ratios are given by $\zeta_1 = \zeta_2 = 0.05$ (Li and Laviage, 2013). The length/width/thickness aspect ratio of the beam is fixed to $100 : 10 : 1$ for all the sample sizes considered. It is worthwhile to mention that, since the beam section is uniform in the axial direction, the trial function given by Eq. (17) is the eigenfunction, and therefore convergence is not an issue in the series discretization even for very small number of modes N. We use $N = 5$ for all the following simulations. Furthermore, since the sample is made of a single layer with doubly symmetric cross-section, it is entirely centrosymmetric. Although PVDF exhibits both piezoelectric and flexoelectric effects, only flexoelectricity is expected to be pronounced in the simulations.

As is known, flexoelectricity only becomes significant at submicron or nanometer scale. So in this work, we set the size of the model to several microns or even smaller. For comparison, two different values for the beam thickness, 3 μm and 0.3 μm, are chosen in the following simulations while keeping the aforementioned length-to-width-to-thickness aspect ratio. All the simulation results are given in forms of frequency response functions (FRFs)

in magnitude form by taking the base acceleration to be the known kinematic input. In other words, we normalized the results by the base acceleration, $\ddot{w}_b = -\omega^2 W_0 e^{j\omega t}$, which is quantified in terms of the gravitational acceleration ($G = 9.81$ m/s^2, not to confuse with the strain gradient coefficient g). We also chose a range of different load resistance values for the simulations to demonstrate the performance of the system under different loadings and identify the optimal electrical load of the maximum power output.

4.1. Voltage FRFs

Fig. 3 shows the voltage output FRFs of a beam with a thickness of 3 μm and the above mentioned aspect ratio (yielding the dimensions of 300 μm × 30 μm × 3 μm). As an expected monotonic trend in energy harvesting, with the increasing load resistance R from 100Ω through 1GΩ, the voltage output also increases. The lowest and highest curves are close to the short-circuit ($R \rightarrow 0$) and open-circuit ($R \rightarrow \infty$) conditions, respectively. It is also observed that the fundamental resonance frequency is insensitive to the load resistance, it maintains a constant value, 7665 Hz, for all the cases. The insensitive behavior of resonance frequency to changing load resistance (from short- to open-circuit conditions) is an indication of very low electromechanical coupling. Note also that the resonance frequency reported here is about 10 times higher than our previous work dealing with piezoelectric energy harvesting at meso-scale even if we are dealing with a softer material. This is an expected result since the resonance frequency increases with decreased specimen size and the specimen we use in the current work is about 100 times smaller than our previous work using meso-scale piezoelectric cantilevers (Erturk, 2012).

If we further shrink the specimen size by 10 times (to have 0.3 μm thickness) to have the dimensions of 30 μm × 3 μm × 0.3 μm and perform the same analysis, the fundamental resonance frequency grows by an order of magnitude as shown in Fig. 4. It is very important to note that, unlike the 3 μm thickness case, the resonance frequency monotonically shifts from 74230 Hz to 75820 Hz with increased load resistance. The amount of change in the resonance frequency as the electrode boundary condition is altered from short- to open-circuit conditions is a measure of electromechanical coupling. This shift was reported previously for piezoelectric energy harvesting using strongly coupled harvesters (DuToit and Wardle, 2007; Erturk and Inman, 2009, 2011). Therefore, comparing Figs. 3 and 4 in terms of the resonance frequency shift reveals substantial improvement in the electromechanical coupling as the sample thickness is reduced from 3 μm to 0.3 μm. Furthermore, since the cantilever is centrosymmetric, the electromechanical coupling is due to flexoelectricity only, and it grows significantly with reduced device thickness. Note that, for a non-centrosymmetric sample that exhibits piezoelectricity,
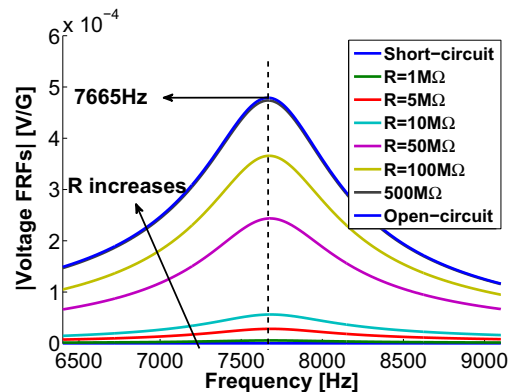

Fig. 3. Voltage FRFs of the centrosymmetric cantilever with 3 μm thickness.

flexoelectric coupling can be comparable to piezoelectric coupling at much smaller thickness levels.

4.2. Tip velocity FRFs

It is more clear to observe the size effect of the proposed flexoelectric energy harvester through the tip velocity FRFs with changing load resistance. As we can see in Fig. 5, there is almost no difference between the curves of various load resistance values for the 3 μm-thick beam case. Therefore, for this thickness level, the flexoelectric coupling is indeed negligible. As a consequence, the effect of vibration attenuation due to the energy dissipation in the resistor (i.e. energy delivered to the load) is negligible for all values of load resistance. It is worth mentioning that the effective bending stiffness incorporating flexoelectric terms is $(EI)^* = (c - \frac{d^2}{a})I_P - \frac{2df}{a}H_P - (\frac{f^2}{a} - g)A_P$, where the relative importance of the terms change with varying sample scale, and H_P is zero for the centrosymmetric sample explored here. For the case of 0.3 μm thickness, as shown in Fig. 6, significant resonance frequency shift (from 74230 Hz to 75820 Hz) is observed, in agreement with the voltage FRFs of this thickness level (Fig. 4). We should emphasize again that the enhancement of the electromechanical coupling with changing thickness level is not the case in piezoelectric transduction. It should be noted that the tip velocity of the harvester is strongly attenuated for certain resistance values, which is due to the shunt damping effect of the resistor i.e. dissipation due to Joule heating. This phenomenon corresponds well with the piezoelectric energy harvesting case in the presence of sufficient electromechanical coupling.

4.3. Power density FRFs

Regarding the size effect observed here, a question is how would we exploit it. One popular measure of the performance of an energy harvester is its power density, i.e. power output per device volume for a given excitation level. The output power here is obtained based on the output voltage by $p(t) = \frac{|v(t)|^2}{R}$. Therefore the power FRFs should be normalized by the square of base acceleration for consistence. The power density FRF is the volumetric density of the power FRF. Figs. 7 and 8 show the power density for the 3 μm and 0.3 μm beams, respectively. As in the case of piezoelectric energy harvesting, the power output does not exhibit monotonic behavior with increasing (or decreasing) the load resistance, revealing the existence of an optimal resistive load at each frequency. Both of the two figures shows maximum output power at $R = 100$ MΩ among the set of resistor considered here, for response around the respective resonance frequencies. Again, we see the resonance frequency shift (from 74230 Hz to 75820 Hz)
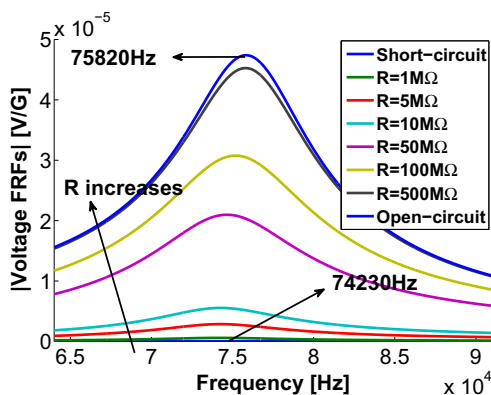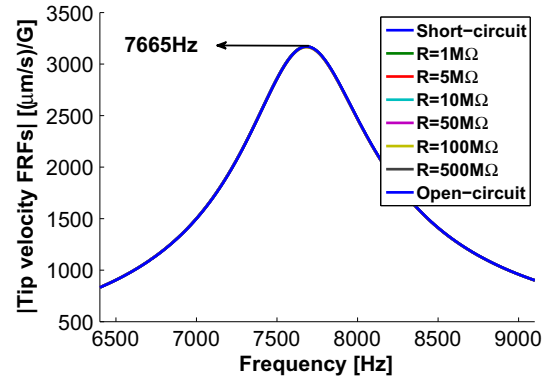

Fig. 5. Tip velocity FRFs of the centrosymmetric cantilever with 3 μm thickness.
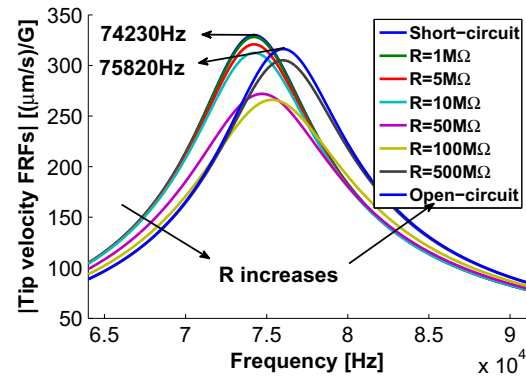

Fig. 6. Tip velocity FRFs of the centrosymmetric cantilever with 0.3 μm thickness.

in 0.3 μm-thickness beam case as the electrical load is changed from short-to open-circuit conditions. The resonance frequency of the maximum power output lies in between these two extremes for a finite non-zero load. The highest curve corresponding to $R = 100$ MΩ shows the resonance frequency of 75180 Hz. It is important to note that there is an increase in the output power density with decreased specimen size. Comparing Figs. 7 and 8, it is found that the maximum output power density for 0.3 μm beam is around 7 times that of the 3 μm beam. Substantial increase in the power density is observed for higher vibration modes as well (not reported here).

4.4. Scaling of the conversion efficiency

To further demonstrate the effect of scaling, we explore the energy conversion efficiency of the flexoelectric energy harvester.
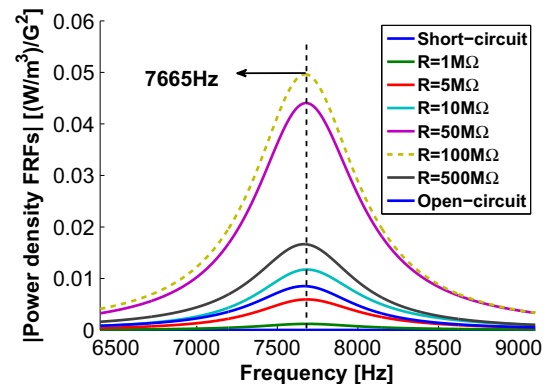

Fig. 4. Voltage FRFs of the centrosymmetric cantilever with 0.3 μm thickness.

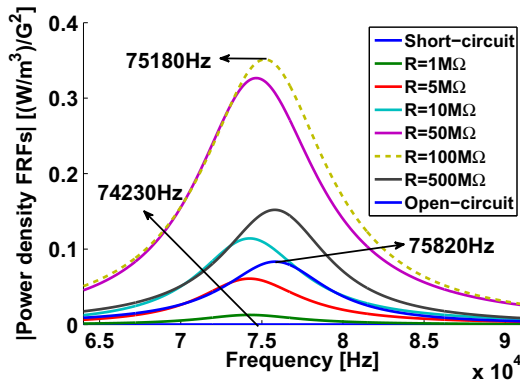**Fig. 7.** Power density FRFs of the centrosymmetric cantilever with 3 μm thickness.

Fig. 8. Power density FRFs of the centrosymmetric cantilever with 0.3 μm thickness.
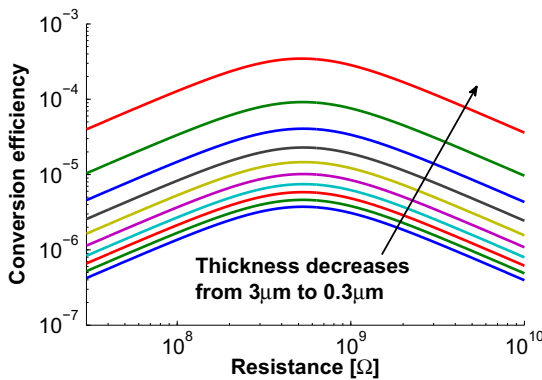

Fig. 9. Resonant energy conversion efficiency for different beam thickness levels (aspect ratio is the same: 100:10:1).

The conversion efficiency is simply the ratio of the electrical power output to the mechanical power input, i.e. the power due to the shear force exerted on the beam by the base. As mentioned previously, the peak electrical power output is $\frac{|v(t)|^2}{R}$. The shear force exerted on the beam by the base is the shear force at $x_1 = 0$, which can be easily expressed by $cI_P \frac{d^3 w(0)}{dx_1^3}$. Therefore the power due to the shear force is the product of the shear force and the base velocity $\frac{dw_b(t)}{dt}$. The mechanical-to-electrical energy conversion efficiency is then

$$\eta = \frac{|v(t)|^2/R}{|cI_P d^3 w(0)/dx_1^3| \cdot |dw_b(t)/dt|} \qquad (25)$$

We maintain the shape of the sample (in terms of the aspect ratio, 100:10:1) and vary the thickness of the beam from 3 μm through 0.3 μm. As shown in Fig. 9, for the 10 different sizes considered in this thickness range, the energy conversion efficiency monotonously increases as the decrease of the sample size. Specifically, the magnitude of the highest curve is about two orders higher than that of the lowest one. Further enhancement in the conversion efficiency can be expected as the beam thickness is reduced to nanometer scale.

5. Conclusions

In this paper, a flexoelectric Euler–Bernoulli model for energy harvesting is proposed following a continuum mathematical framework accounting for the two-way flexoelectric coupling. Linear constitutive law is used for describing the elastic, dielectric,

and flexoelectric behavior of the material. Based on the variational principle for flexoelectricity, the Euler–Lagrange equations are derived. A generalized assumed-modes method is employed for the solution of the governing equations and frequency–response simulations of technologically relevant case studies. In contrast to piezoelectricity, a single centrosymmetric beam may be used for generating electricity through flexoelectricity. In this work, it is shown that the easily fabricated, simple symmetric thin beam serves as a good candidate for the flexoelectric energy harvester at sub-micron scales. Since flexoelectricity, unlike piezoelectricity, is universally present in all dielectrics, including amorphous materials, the current work may be useful for exploring energy harvesting in a wide variety of materials including soft biomaterials. Finally, we have shown a substantial size effect in flexoelectric energy harvesting. A two orders of magnitude increase in the mechanical-to-electrical energy conversion efficiency is shown due to the reduction of the sample's thickness from 3 μm to 0.3 μm. Due to the this size effect, the proposed flexoelectric energy harvester is likely to be more attractive for micro and nano-scale devices.

Acknowledgement

References

Anton, S.R., Sodano, H.A., 2007. A review of power harvesting using piezoelectric materials (2003–2006). Smart Mater. Struct. 16, R1–R21.

Anton, S.R., Erturk, A., Inman, D.J., 2012. Multifunctional unmanned aerial vehicle wing spar for low-power generation and storage. AIAA J. Aircr. 49, 292–301.

Brownell, W.E., Spector, A.A., Raphael, R.M., Popel, A.S., 2001. Micro- and nanomechanics of the cochlear outer hair cell. Ann. Rev. Biomed. Eng. 3, 169–194.

Brownell, W.E., Farrell, B., Raphael, R.M., 2003. Membrane electromechanics at hair-cell synapses. Biophysics of the Cochlea: from Molecules to Models, pp. 169–176.

Carl, K., 1975. Ferroelectric properties and fatigue effects of modified PbTiO ceramics. Ferroelectrics 9, 23.

Catalan, G., Sinnamon, L.J., Gregg, J.M., 2004. The effect of flexoelectricity on the dielectric properties of inhomogeneously strained ferroelectric thin films. J. Phys.: Condens. Matter 16 (13), 2253–2264.

Chu, B., Salem, D.R., 2012. Flexoelectricity in several thermoplastic and thermosetting polymers. Appl. Phys. Lett. 101, 103905.

Clough, R.M., Penzien, J., 1993. Dynamics of Structures, 2nd ed. McGraw Hill, New York.

Cook-Chennault, K.A., Thambi, N., Sastry, A.M., 2008. Powering MEMS portable devices-a review of non-regenerative and regenerative power supply systems with emphasis on piezoelectric energy harvesting systems. Smart Mater. Struct. 17, 043001.

Cross, L.E., 2006. Flexoelectric effects: charge separation in insulating solids subjected to elastic strain gradients. J. Mater. Sci. 41, 53–63.

Deng, Q., Liu, L., Sharma, P., 2014. Flexoelectricity in soft materials and biological membranes. J. Mech. Phys. Solids 62, 209–227.

Dorfmann, A., Ogden, R.W., 2005. Nonlinear electroelasticity. Acta Mech. 174, 167–183.

Dumitrica, T., Landis, C.M., Yakobson, B.I., 2002. Curvature induced polarization in carbon nanoshells. Chem. Phys. Lett. 360 (1–2), 182–188.

DuToit, N.E., Wardle, B.L., 2007. Experimental verification of models for microfabricated piezoelectric vibration energy harvesters. AIAA J. 45 (5), 1126–1137.

Eliseev, E.A., Morozovska, A.N., Glinchuk, M.D., Blinc, R., 2009. Spontaneous flexoelectric/flexomagnetic effect in nanoferroics. Phys. Rev. B 79, 165433.

Eliseev, E.A., Glinchuk, M.D., Khist, V., Skorokhod, V.V., Blinc, R., Morozovska, A.N., 2011. Linear magnetoelectric coupling and ferroelectricity induced by the flexomagnetic effect in ferroics. Phys. Rev. B 84, 174112.

Elvin, N., Erturk, A., 2013. Advances in Energy Harvesting Methods. Springer, New York.

Eringen, A.C., Maugin, G.A., 1990. Electrodynamics of Continua, vol. I and II. Springer press, New York.

Erturk, A., 2012. Assumed-modes modeling of piezoelectric energy harvesters: Euler–Bernoulli, Rayleigh, and Timoshenko models with axial deformations. Comput. Struct. 106107, 214–227.

Erturk, A., Inman, D.J., 2009. An experimentally validated bimorph cantilever model for piezoelectric energy harvesting from base excitations. Smart Mater. Struct. 18, 025009.

Erturk, A., Inman, D.J., 2011. Piezoelectric Energy Harvesting. Wiley.

Fu, J.Y., Zhu, W., Li, N., Cross, L.E., 2006. Experimental studies of the converse flexoelectric effect induced by inhomogeneous electric field in a barium strontium titanate composition. J. Appl. Phys. 100, 024112.

Fu, J.Y., Zhu, W., Li, N., Smith, N.B., Cross, L.E., 2007. Gradient scaling phenomenon in microsize flexoelectric piezoelectric composites. Appl. Phys. Lett. 91, 182910.

Gharbi, M., Sun, Z.H., Sharma, P., White, K., El-Borgi, S., 2011. Flexoelectric properties of ferroelectrics and the nanoindentation size-effect. Int. J. Solids Struct. 48, 249.

Guney, H.Y., 2005. Elastic properties and mechanical relaxation behaviors of PVDF (poly (vinylidene fluoride)) at temperatures between −20 and 100 °C and at 2 MHz ultrasonic frequency. J. Polym. Sci. Polym. Phys. 43, 2862–2873.

Hudak, N.S., Amatucci, G.G., 2008. Small-scale energy harvesting through thermoelectric, vibration, and radiofrequency power conversion. J. Appl. Phys. 103 (10), 101301.

Jeon, Y., 2005. MEMS power generator with transverse mode thin film PZT. Sens. Actuators A: Phys. 122 (1), 16–22.

Jiang, Q., Cao, W., Cross, L.E., 1994. Electric fatigue in lead zirconate titanate ceramics. J. Am. Ceram. Soc. 77, 211.

Kalinin, S.V., Meunier, V., 2008. Electronic flexoelectricity in low-dimensional systems. Phys. Rev. B 77 (3), 033403-1–033403-4.

Kymissis, J., Kendall, C., Paradiso, J., Gershenfeld, N., Parasitic power harvesting shoes. In: Proc. 2nd IEEE Int. Conf. Wearable Computing (California), pp. 132–139, 1998.

Li, B., Laviage, A.J., You, J.H., Kimb, Y.J., 2013. Harvesting low-frequency acoustic energy using multiple PVDF beam arrays in quarter-wavelength acoustic resonator. Appl. Acoust. 74, 1271–1278.

Liu, L., 2014. An energy formulation of continuum magneto-electro-elasticity with applications. J. Mech. Phys. Solids 63, 451–480.

Ma, W., Cross, L.E., 2001. Large flexoelectric polarization in ceramic lead magnesium niobate. Appl. Phys. Lett. 79 (19), 4420–4422.

Ma, W., Cross, L.E., 2002. Flexoelectric polarization in barium strontium titanate in the paraelectric state. Appl. Phys. Lett. 81 (19), 3440–3442.

Ma, W., Cross, L.E., 2003. Strain-gradient induced electric polarization in lead zirconate titanate ceramics. Appl. Phys. Lett. 82 (19), 3923–3925.

Ma, W., Cross, L.E., 2006. Flexoelectricity of barium titanate. Appl. Phys. Lett. 88, 232902.

Majdoub, M.S., Sharma, P., Cagin, T., 2008a. Enhanced size-dependent piezoelectricity and elasticity in nanostructures due to the flexoelectric effect. Phys. Rev. B 77, 125424-1.

Majdoub, M.S., Sharma, P., Cagin, T., 2008b. Dramatic enhancement in energy harvesting for a narrow range of dimensions in piezoelectric nanostructures. Phys. Rev. B 78, 121407(R).

Majdoub, M.S., Maranganti, R., Sharma, P., 2009a. Understanding the origins of the intrinsic dead layer effect in nanocapacitors. Phys. Rev. B 79, 115412.

Majdoub, M.S., Sharma, P., Cagin, T., 2009b. Erratum: enhanced size-dependent piezoelectricity and elasticity in nanostructures due to the flexoelectric effect. Phys. Rev. B 79, 119904(E).

Majdoub, M.S., Sharma, P., Cagin, T., 2009c. Erratum: dramatic enhancement in energy harvesting for a narrow range of dimensions in piezoelectric nanostructures. Phys. Rev. B 79, 159901(E).

Maranganti, R., Sharma, P., 2009. Atomistic determination of flexoelectric properties of crystalline dielectrics. Phys. Rev. B 80, 054109.

Maranganti, R., Sharma, N.D., Sharma, P., 2006. Electromechanical coupling in nonpiezoelectric materials due to nanoscale nonlocal size effects: Green's function solutions and embedded inclusions. Phys. Rev. B 74, 014110.

McMeeking, R.M., Landis, C.M., 2005. Electrostatic forces and stored energy for deformable dielectric materials. J. Appl. Mech. 72, 581–590.

Meirovitch, L., 2001. Fundamentals of Vibrations. McGraw Hill, New York.

Mindlin, R.D., 1961. On the equations of motion of piezoelectric crystals. In: Problems of Continuum Mechanics. Society for Industrial and Applied Mathematics, Philadelphia, pp. 282–290.

Mindlin, R.D., 1968. Polarization gradient in elastic dielectrics. Int. J. Solids Struct. 4, 637–642.

Muralt, P., Polcawich, R., Trolier-McKinstry, S., 2009. Piezoelectric thin films for sensors, actuators, and energy harvesting. MRS Bulletin 34 (09), 658–664.

Murayama, N., Nakamura, K., Obara, H., Segawa, M., 1976. The strong piezoelectricity in polyvinylidene fluoride (PVDF). Ultrasonics 14 (1), 15–24.

Nguyen, T.D., Mao, S., Yeh, Y.W., Purohit, P.K., 2013. MC McAlpine nanoscale flexoelectricity. Adv. Mater. 25 (7), 946.

Priya, S., 2007. Advances in energy harvesting using low profile piezoelectric transducers. J. Electroceram. 19, 167–184.

Quarrie, M., 1953. Time effects in the hysteresis loop of polycrystalline barium titanate. J. Appl. Phys. 24, 1334.

Raphael, R.M., Popel, A.S., Brownell, W.E., 2000. A membrane bending model of outer hair cell electromotility. Biophys. J. 78 (6), 2844–2862.

Sahin, E., Dost, S., 1988. A strain-gradients theory of elastic dielectrics with spatial dispersion. Int. J. Eng. Sci. 26 (12), 1231–1245.

Salaneck, W.R., 1972. Some fatigue effects in 8/65/35 PLZT fine grained ferroelectric ceramics. Ferroelectrics 4, 97.

Sharma, N.D., Maranganti, R., Sharma, P., 2007. On the possibility of piezoelectric nanocomposites without using piezoelectric materials. J. Mech. Phys. Solids 55, 2328–2350.

Sharma, N.D., Landis, C.M., Sharma, P., 2010. Piezoelectric thin-film superlattices without using piezoelectric materials. J. Appl. Phys. 108, 024304.

Sharma, N.D., Landis, C.M., Sharma, P., 2012. Erratum: Piezoelectric thin-film super-lattices without using piezoelectric materials [J. Appl. Phys. 108, 024304 (2010)]. J. Appl. Phys. 111, 059901.

Shenck, N.S., Paradiso, J.A., 2001. Energy scavenging with shoe-mounted piezoelectrics. IEEE Micro 21, 30–42.

Steigmann, D.J., 2009. On the formulation of balance laws for electromagnetic continua. Math. Mech. Solids 14 (4), 390–402.

Suo, Z., Zhao, X., Greene, W., 2008. A nonlinear field theory of deformable dielectrics. J. Mech. Phys. Solids 56, 467–486.

Tagantsev, A.K., 1986. Piezoelectricity and flexoelectricity in crystalline dielectrics. Phys. Rev. B 34, 5883–5889.

Tagantsev, A.K., Meunier, V., Sharma, P., 2009. Novel electromechanical phenomena at the nanoscale: phenomenological theory and atomistic modeling. MRS Bulletin 34 (9), 643–647.

Tiersten, H.F., 1967. Hamilton's principle for linear piezoelectric media. Proc. IEEE – PIEEE 55 (8), 1523–1524.

Toupin, R.A., 1956. The elastic dielectric. J. Ration. Mech. Anal. 5, 849–915.

Trolier-McKinstry, S., Muralt, P., 2004. Thin film piezoelectrics for MEMS. J. Electroceram. 12 (1–2), 7–17.

Wang, Z.L., Song, J., 2006. Piezoelectric nanogenerators based on zinc oxide nanowire arrays. Science 312 (5771), 242–246.

Williams, R., 1965. Surface layer and decay of the switching properties of barium titanate. J. Phys. Chem. Solids 26, 399–405.

Xu, S. et al., 2010. Self-powered nanowire devices. Nat. Nanotechnol. 5 (5), 366–373.

Zubko, P., Catalan, G., Buckley, A., Welche, P.R.L., Scott, J.F., 2007. Strain-gradient induced polarization in SrTio$_3$ single crystals. Phys. Rev. Lett. 99, 167601.